Front. Chem. China 2011, 6(4): 341–354
DOI 10.1007/s11458-011-0258-1

REVIEW ARTICLE

Surface-enhanced Raman scattering (SERS) based on surface plasmon resonance coupling techniques

Shuping XU, Yu LIU, Haibo LI
and Weiqing XU (✉)

Surface plasmon resonance (SPR) can provide a remarkably enhanced electromagetic field around metal surface. It is one of the enhancement models for explaining surface-enhanced Raman scattering (SERS) phonomenon. With the development of SERS theories and techniques, more and more studies referred to the configurations of the optical devices for coupling the excitation and radiation of SERS, including the prism-coupling, waveguide-coupling, and grating-coupling modes. In this review, we will summarize the recent experimental improvements on the surface plasmon-coupled SERS.

Keywords surface-enhanced Raman scattering (SERS), electromagnetic field, surface plasmon resonance (SPR), metal film, grating

1 Introduction

Raman spectroscopy is one of the crucial analytical techniques for the characterization of molecular structures in a nondestructive manner. However, normal Raman signal is usually low, which limits its applications in many fields. The discovery of surface-enhanced Raman scattering (SERS) and surface-enhanced resonance Raman scattering (SERRS) overcome the drawbacks of normal Raman [1–7]. SERS brings million-fold enhancement of Raman signals, which makes great strides in the applications of Raman spectroscopy [8,9]. SERS spectroscopy has been proved to be successful in achieving the single-molecule detection level by Nie [10], Kneipp [11] and Xu [12]. Since then, more and more researchers become interested in this unusual spectral phenomenon and its theory is becoming explicit.

Studies on the electromagnetic (EM) mechanism of SERS find that SERS is closely related to the surface plasmons (SPs) of metal. The SPs refer to the collectively oscillated free electrons which pinned to the interface between a metal and a dielectric medium. Due to the boundary conditions of electric fields in different metal structures, the SPs can be divided into the propagating surface plasmons (PSPs) which propagate on the interface of metal/dielectric medium and the localized surface plasmons (LSPs) which are located in metal nanoparticles or nano structures. The SPs interact with the EM field, which can enhance the EM field and further improve the spectral signals of the photo-active molecules involved in this EM field. In addition, the SPs can re-couple with the photons radiated from molecules, resulting in spectral radiation in a certain direction. So far, besides SERS, the SPR effect was employed to explain many spectral phenomena, such as, plasmon-controlled fluorescence [13–15], surface-enhanced infrared spectroscopy (SE-IR) [16], super transmission effect (super lens) [17], etc.

The effective coupling of SPs is considered to be a key point for achieving the huge enhancement of SERS[18–21]. The strategies for the LSPR- and PSPR-coupled SERS are varied.

The tuning of LSPR bands to match the excited light by the morphologies of selective metal nanoparticles was a main approach for the LSPR coupling modes. The vast majority of experimental results were carried out through a statistical result of a great deal of metal nanoaggregates [22–24]. Besides this, the excitation wavelength of laser is considered to be an important tunable parameter to match the LSPR bands of metal structures. The wavelength dependent-SERS spectra disclosed that the maximum SERS enhancement factor (EF) occurs when the excitation wavelengths are blue-shifted with respect to the LSPR bands of metal substrates [25]. Moreover, near-field techniques, such as high numerical aperture (NA) lens [26–28], and metal cantilever tips [29–31] etc., have been well designed for the LSPR-coupled SERS.

To best couple SPs, many optical configurations and devices were designed and assembled, such as, prism, grating and waveguide. Since the wave-vector of PSPs is lower than that of the incident light, SPs cannot be directly excited if incident light shines in a metal surface. By using a coupling device, the wave-vector of the incident light can be tuned and can match the SPs' wave-vector. Experimental factors in these SPR configurations, such as, excitation wavelength, incident and detection angles, thickness of metal film, and etc. decide the coupling efficiency of the incident light and SPs. Therefore the optimization of these factors is very important to obtain strong SERS. In this review, we will particularize the coupling techniques of the SP-coupled SERS according to different optical devices.

Received October 26, 2011; accepted November 2, 2011
State Key Laboratory of Supramolecular Structure and Materials, Jilin University, Changchun 130012, China
E-mail: xuwq@jlu.edu.cn

2 SERS based on the evanescent field excitation

Many optical devices for SERS were designed based on the evanescent field excitation mode. In a multilayer system with metal, when the excitation beam goes from an optically denser medium to a thinner medium as an incident angle larger than the total reflection angle, the total reflection occurs at the interface of two mediums. At the point where the total internal reflection occurs, the evanescent wave caused by incident light can penetrate into the sample layer through the metal layer and excite the SERS of analytes adsorbed on metal. The evanescent wave from the point of incidence to the thinner medium attenuates as the penetration depth increases. Finally, it disappears. If the metal layer is not taken into account, the penetration depth of the evanescent wave (d_p) can be determined by the refractive indices of two mediums (n_1 and n_1) and the incident angle (α). Their relationship is given by the following formula (1):

$$d_p = \frac{\lambda}{2\pi n_1 \cdot [\cos^2\alpha - (n_2/n_1)^2]^{1/2}} \quad (1)$$

where λ is the wavelength of incident light.

Two representative configurations using the evanescent field excitation mode are shown, which are the prism-coupling and waveguide-coupling SERS.

2.1 SERS based on prism-coupling SPR configurations

A prism modified with a thin metal film is a basic structure for the prism-coupling SPR sensors. Two kinds of prisms were commonly used, Otto and Kretschmann types. In an Otto-type SPR, there is an air layer between the metal film and prism. Since it is still a challenge to control the thickness of the air layer in the experimental condition, the Otto-type SPR has been seldom employed. More and more recent studies adopted the Kretschmann type prisms to design the SP-coupled SERS setups.

For a multilayer composited SPR setup (Fig. 1), the media between a high refractive prism and a semi-infinitely dielectric substrate can be considered as a stratified medium. The dielectric constants of the transparent prism and semi-infinitely dielectric substrate are ε_p and ε_s. The jth layer of the stratified medium has a thickness of d_j and a complex dielectric constant of ε_j. When an incident plane light-wave goes through the transparent prism and falls on the boundary between the prism and multilayer medium with an incidence angle of θ, it split into two: the reflecting wave in prism and the transmitted wave in multilayer medium. It is assumed that the transmittance (T) equals zero under the attenuated total reflection (ATR) condition. If no other energy is missing, the reflectance (R) is given by Eq. (2) [32,33]:

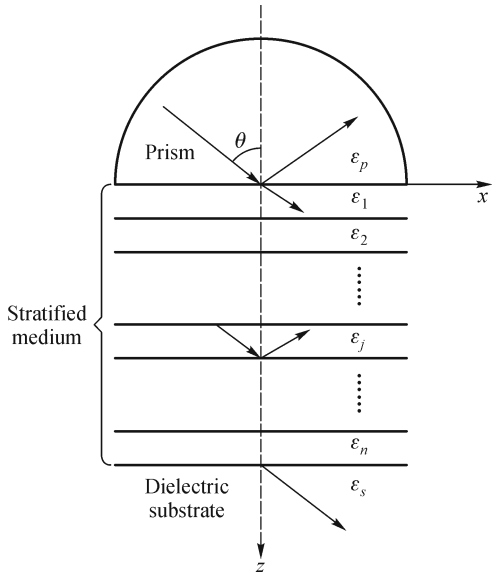

Figure 1 Interaction of a plane wave in a stratified medium system

$$R = 1 - A = 1 - \left(\frac{2\pi}{\lambda}\right)^2 \frac{1}{k_{zp}} \sum_{j=1}^{N} \int_{Z_j}^{Z_{j+1}} \mathrm{Im}(\varepsilon_j) \left\langle E_{//z}^2 \right\rangle \mathrm{d}z \quad (2)$$

For a simple prism/metal film/dielectric medium tirlayer system, if the dielectric substrate is nonabsorbing medium, only metal film is the absorbing medium. The reflectance can be expressed by Eq. (3):

$$R = 1 - A = 1 - \left(\frac{2\pi}{\lambda}\right)^2 \frac{1}{k_{zp}} \int_0^{d_M} \mathrm{Im}(\varepsilon_M) \left\langle E_{//z}^2 \right\rangle \mathrm{d}z \quad (3)$$

When a p-polarized incident beam falls on the prism/metal film interface with the angle of incident in the vicinity of the SPR angle, the free electrons on the metal film surface respond collectively by oscillating in resonance with the light wave. The electronic field at the resonant condition can be expressed by Eqs. (4) and (5):

$$\left\langle E_{x,z=d_{M^+}}^2 \right\rangle = |\varepsilon_p| \left| \frac{k_{zs}}{(2\pi/\lambda)\varepsilon_s} t_{//} \right|^2 \quad (4)$$

$$\left\langle E_{z,z=d_{M^+}}^2 \right\rangle = \left| \frac{k_{xp}}{(2\pi/\lambda)\varepsilon_s} t_{//} \right|^2 \quad (5)$$

The resonance interaction between the electromagnetic field of the light and the surface charge oscillation leads to intensive absorption of incident light by the absorbing medium. Also, under the resonance angle excitation, the strongest EM was provided, which exciteed the highest SERS signals of adsorbed analytes [34]. So in the prism-coupling

SPR configurations, the optimization of the SP coupling for SERS excitation is usually through tuning the incident and detection angles to the SPR angle.

The report written by Giergie and Hemminger [35] summarized four possible ways to detect SERS by Kretschmann type prisms, and three of four optical arrangements (a, b and c) had been proved to be feasible. They prospected by the theoretical calculations that there would be a ~1000-fold increase in the Raman intensity relative to the optimized backscattering geometry from three terms: electric field enhancement by incident field, radiation increase of Raman scatterers and Raman collection efficiency improvement by using typical collection optics.

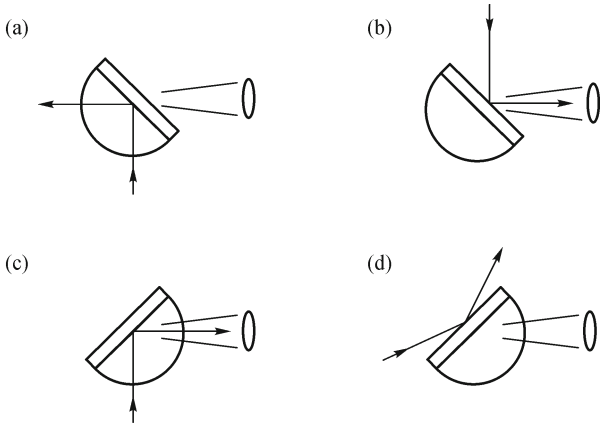

Figure 2 The four possible ways to measure Raman scattering using a Kretschmann prism. Reprinted with permission from Ref. [35]. Copyright©1988 American Chemical Society

SERS detection from evanescent field in a Kretschmann type prism configuration was provided by Chen et al. [36] and Xu et al. [37]. Chen presented an optical device capable of the simultaneous measurement of the SPR and SERS spectra for direct real-time analysis of biomolecular interactions, e.g., the protein structural changes [38], DNA [39]. They adopted the attenuated total reflection (ATR) method with an Au nanoclusters-embedded dielectric sensing film to construct the SPR and SERS sensing techniques. The sub-micro molarity of DNA concentration was achieved by using this ATR-SPR/SERS method.

A SPR-SERS spectrometer developed by Xu et al. [37] collects SERS signals and images in the evanescent field (see Fig. 4). The imaging system works for the system modulation, which assures the SPR and SERS spectra originated from a same spot. The SPR detection has no influence on the SERS measurement. Moreover, the incident light and SERS collection systems lie in different sides of the prism, which can avoid the interference of the incident light. The SPR-SERS microspectrometer is composed of three main functional parts: an incident light system, an SPR detection system

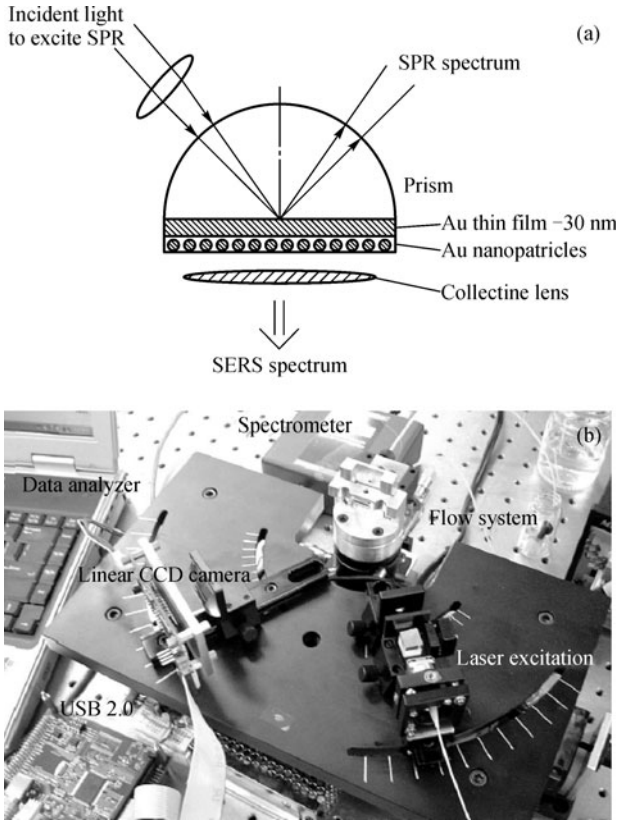

Figure 3 (a) ATR-SPR/SERS optical setup with gold nanoparticle enhancement; (b) Photograph of ATR-SPR/SERS device. Reprinted with permission from Ref. [36]. Copyright©2004 SPIE

and an SERS detection system (Fig. 4). When an incident beam was focused on the surface of metal film, part of the incident beams were reflected and then collected by the SPR detection system. At the same time, the Raman scattering of analytes was excited as well, which was collected by the SERS detection system via an inverted microscope. This SPR-SERS instrument was employed for the angle-dependent SPR and SERS spectra. It was applied for the following three examples (Fig. 5).

By using this SPR-SERS instrument, the SPR and SERS of 4-aminothiophenol (4-ATP) and 4-mercaptopyridine (4-Mpy) was simultaneously measured. Fig. 6(a) is the incident angle-dependent SERS spectra of 4-Mpy in air. The SERS peak intensity as a function of incident angle was plotted (Fig. 6(b)). It is found that the maximal SERS signals appeared at the vicinity of the SPR angle (Fig. 6(b)). SERS intensity acquired under resonance angle excitation was about 8 times higher than that acquired under non-resonance condition. The EF was evaluated to be about 2.0×10^6 for 4-Mpy [37]. The SPR bands can be tuned by different dielectric mediums and prisms. The SPR angle and SERS angle (the angle with the maximum SERS) shifted to higher degrees as the refractive indices of dielectric mediums increased.

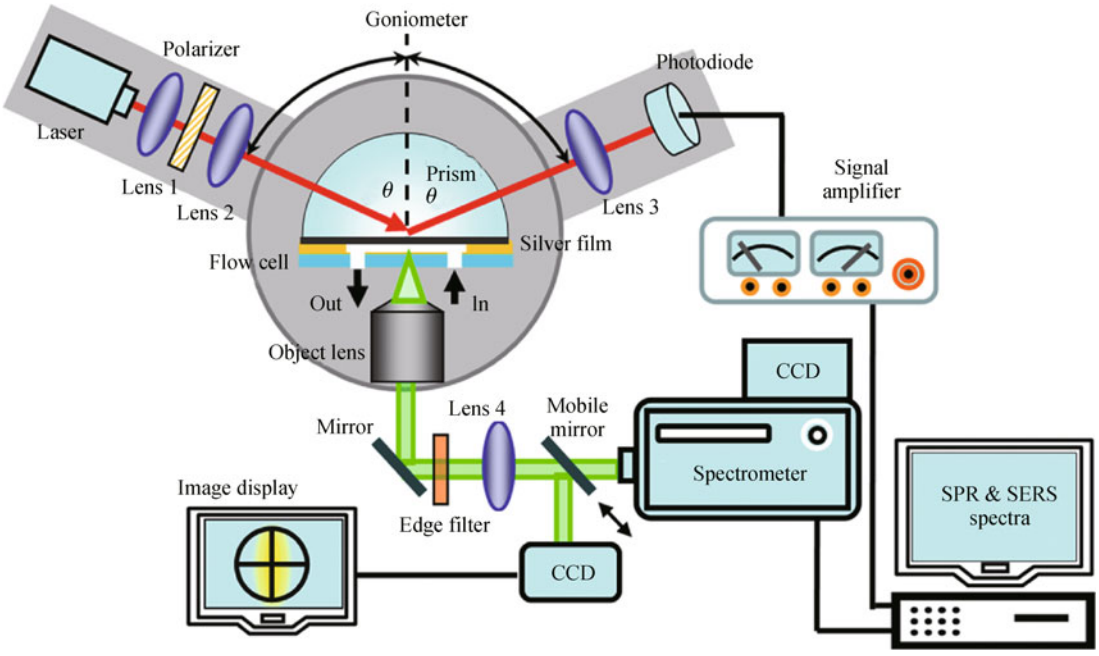

Figure 4 The schematic diagram of SPR-SERS microspectrometer. Reprinted with permission from Ref. [37]. Copyright 2010 American Institute of Physics

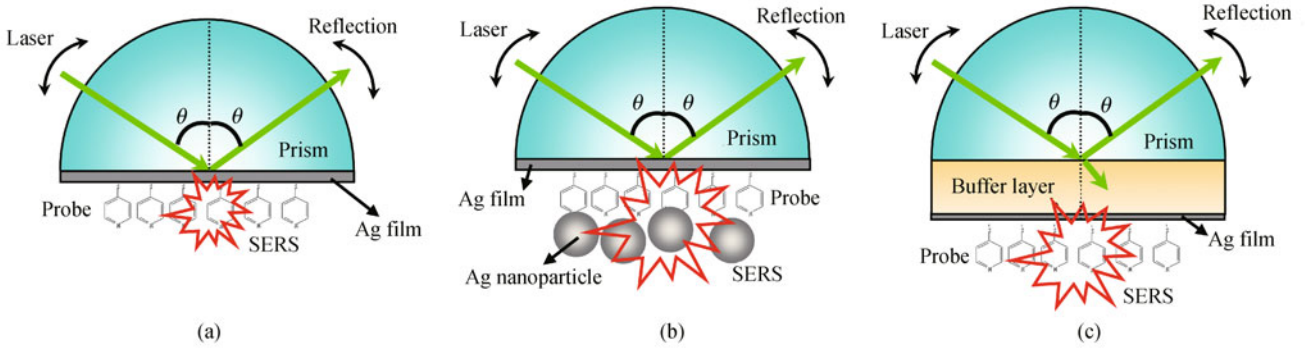

Figure 5 The schematic diagram of SERS spectroscopies based on (a) propagating SP excitation, (b) localized and propagating SP co-enhancement, and (c) long-range SP excitation

Figures 7 (a) and (b) compared the SPR coupled SERS based on the evanescent field excitation and bright field excitation. From the SERS spectra (Fig. 7(c)), it can be found that the evanescent field excitation mode resulted in a higher signal/noise ratio. The background signal in the spectra of the evanescent field excitation had been compressed effectively.

Theoretical prediction shows that the SERS excited by PSPs is supposed to be very low, providing 10^2–10^5 fold enhancement under the resonance condition [40,41]. Through introducing LSPs involved in the PSPs system, SERS signals can be further improved [42–45]. Fig. 8 (a) shows the SPR curves and the SERS intensity profile obtained on two kinds of substrates (Figs. 5 (a) and (b)) [46]. Metal nanoparticles were employed to increase the LSPs' contribution in a hope to acquire stronger SERS signals. The electric field at the gap between the silver film and a silver nanoparticle increased about 4000 times according to the simulation result [46]. The SERS signal (at 1573 cm^{-1}) obtained under the LSP-PSP co-enhancement (upper spectrum) was 55 times above the signal obtained on the vacuum-deposited silver film (bottom spectrum). The EF was estimated to be as large as 2.0×10^7.

Long-range surface plasmon (LRSP) is a special type of PSP—a surface electromagnetic wave which originates from a thin metal film embedded in two dielectric layers. In a prism-coupling configuration, LRSPs possess longer surface propagation lengths, higher surface electric field strengths, narrower angular resonance curves, and lower resonance

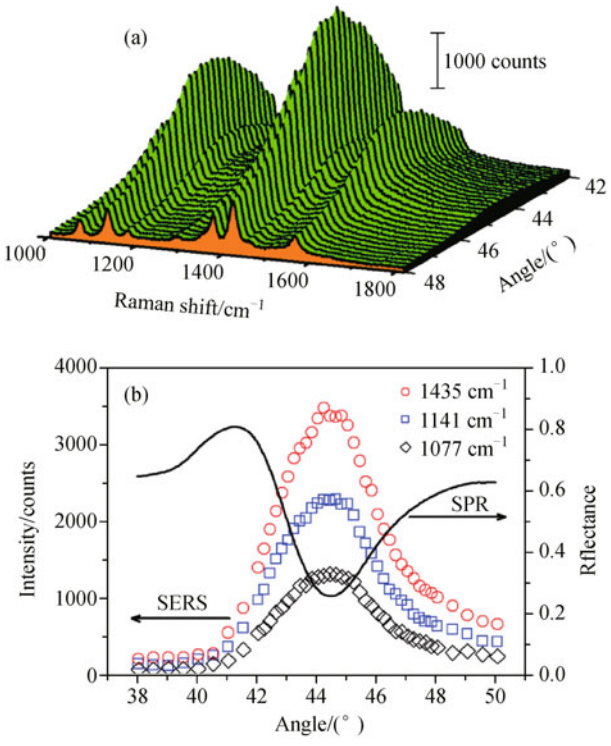

Figure 6 (a) The incident angle-dependent SERS spectra of 4-ATP. The integration time of all SERS spectra was 10 s and the laser power was 8 mW. (b) The SERS peak intensities of the 4-ATP at 1435 (○), 1141 (□), and 1077 cm^{-1} (◇) are plotted with the incident angles. The SPR curve was recorded as the interval of 0.02°. Reprinted with permission from Ref. [37]. Copyright©2010 American Institute of Physics

angle compared with the conventional SPs [47–54]. A new SERS excitation strategy in the evanescent field by the LRSPs was proposed to further increase the SERS signals [55]. A four-phase Kretschmann LRSPR setup composed of a prism/MgF_2 film/silver film/water configuration was built (Fig. 5(c)). Incident angle-dependent SERS spectra were measured in the evanescent field on this four-phase configuration. The SERS signals obtained under the evanescent field excitation at the LRSPR angle were 15 times higher than that collected based on the conventional SPR configuration (Fig. 9). The experimental result proved that the penetration depth of LRSPs was at least 500 nm, which was longer than the electric field penetration depth of conventional SPs. The LRSPs offer a number of important advantages for Raman excitation. One important aspect is that the angle distribution of the electric field at the metal/dielectric interface becomes narrow, which is more effective for SERS excitation and signal detection. Moreover, the penetration depth of LRSPs was larger than that of normal SPs, which could excite more probe molecule and widen the SERS applications in multilayer systems.

ATR method is a classic method to excite the surface plasmon polaritons (SPPs) and to achieve with ease the directional coupled emission of SPs. Earlier researches have proved that ATR approach in a prism is a feasible configuration for pumping SERS. Futamata et al. [56–58] reported a SERS setup based on an Otto prism configuration (Fig. 10). A Weierstrass prism and two objectives were used to alternatively collect the reflective and Raman scattering lights from the same direction. By using this setup, they studied the SERS intensity at different incident (detection) angles and proved that the ATR-mode SERS spectroscopy is very useful in improving the signal sensitivity.

Recently, Etchegoin et al. [59] showed their design on the simultaneous measurement of SPR and SERS in a back-scattering mode by using a Kretschmann prism (Fig. 11). They used the back focal plane illumination to improve the coupling to resonance. The maximal coupling of the beam with SPPs happened at the resonance angles, which were wavelength-dependant. A high angular resolution with good collection efficiency was combined. Molecules were excited at the resonance angle while the Raman-shifted lights were mostly concentrated at a very similar angle but in any

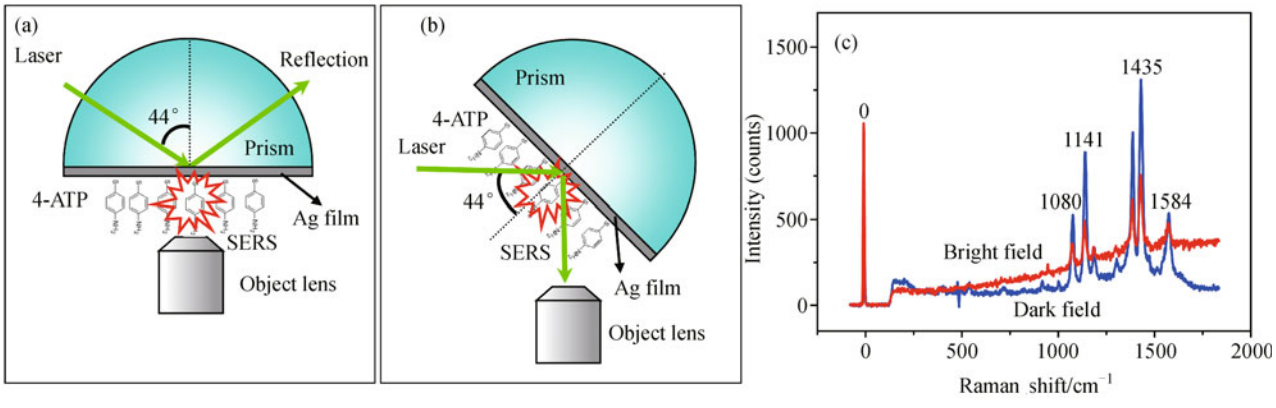

Figure 7 The schematic diagram of the SP-enhanced SERS based on (a) the evanescent field excitation and (b) bright field excitation. (c) The SERS spectra excited via the evanescent field and bright field. The incident angle was 44°.

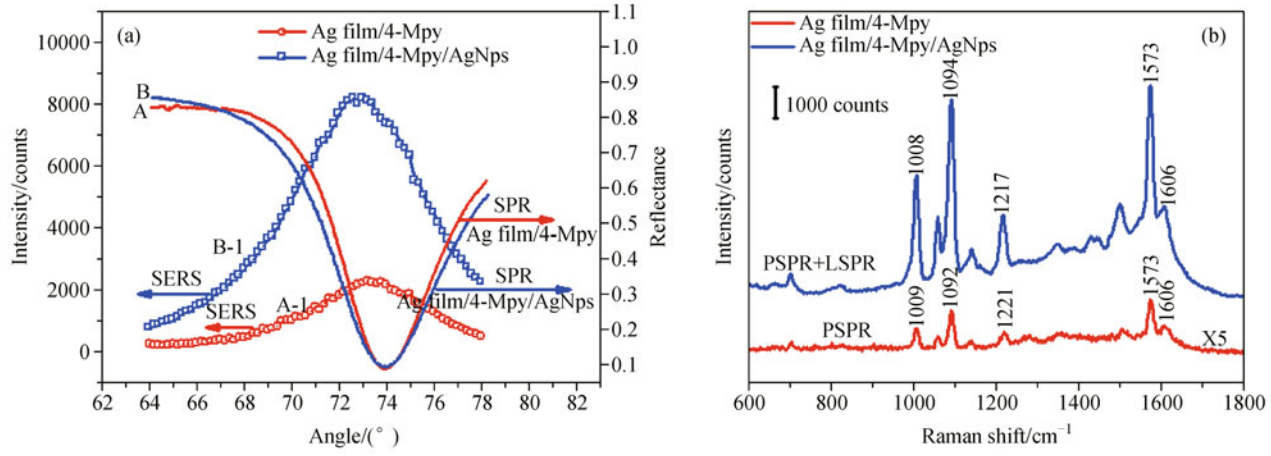

Figure 8 (a) Curve A and A-1 are the SPR curve and SERS intensity profile of 4-Mpy on a vacuum-deposited silver film. Curve B and B-1 are the SPR curve and SERS intensity profile of 4-Mpy under the LSP-PSP co-enhancement. (b) The strongest SERS spectra of 4-Mpy on a silver film and a sandwich structure excited under the resonance condition. Reprinted with permission from Ref. [46]. Copyright©2011 Royal Society of Chemistry

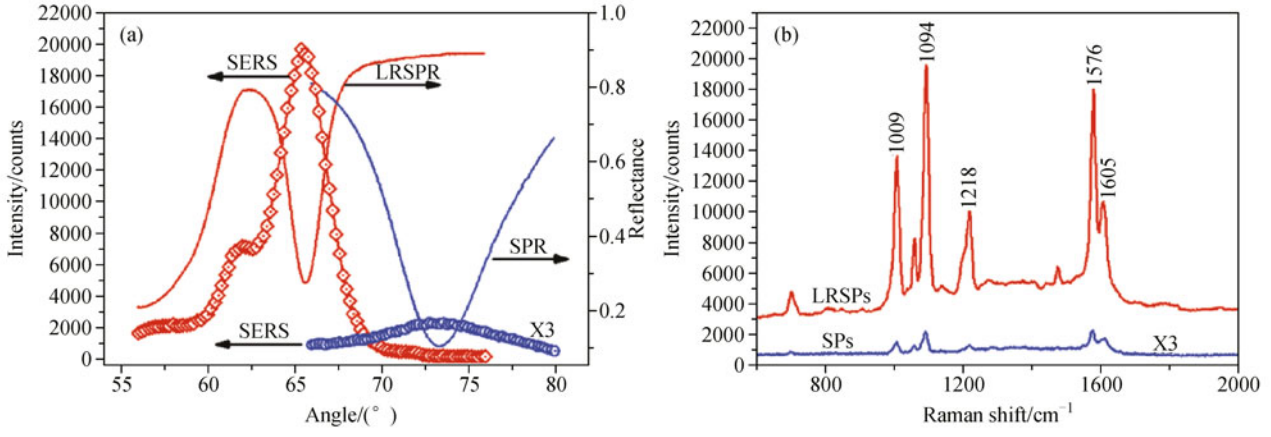

Figure 9 (a) A comparison of the angular reflectivity scans recorded on a normal SPR configuration and a LRSPR configuration. The angle-dependent SP field-enhanced SERS intensities under a SPR configuration (○) and a LRSPR configuration (◇) were also shown. (b) The SERS spectra excited by the LRSPs at the resonance angles of 65.4° (top curve) and the SPs at the resonance angles of 72° (bottom curve). Reprinted with permission from Ref. [55]. Copyright©2011 American Chemical Society

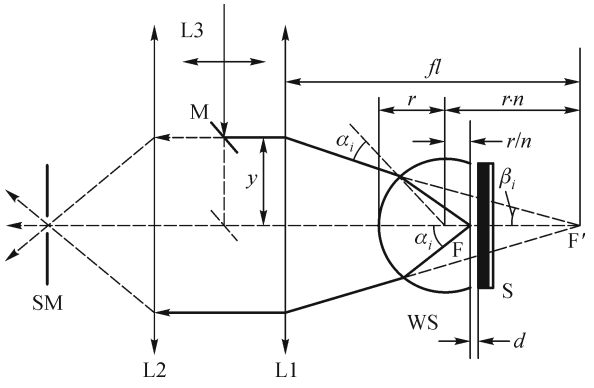

Figure 10 Schematic light scattering configuration in ATR-SPP resonance with the weierstrass prism. Reprinted with permission from Ref. [58]. Copyright©1995 American Chemical Society

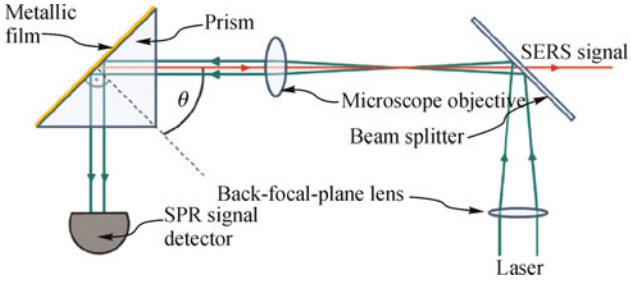

Figure 11 Schematics of the optical setup for combined SPR-SERS in a backscattering configuration. Reprinted with permission from Ref. [59]. Copyright©2011 American Chemical Society

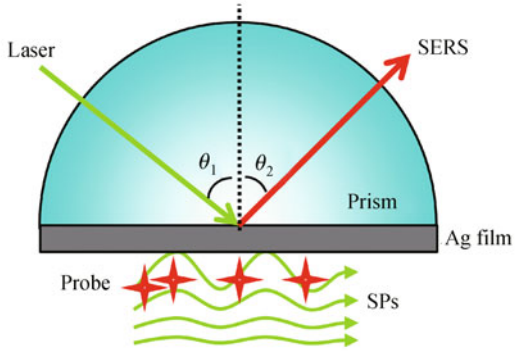

Figure 12 The design of the directional SERS based on back coupled radiation mode

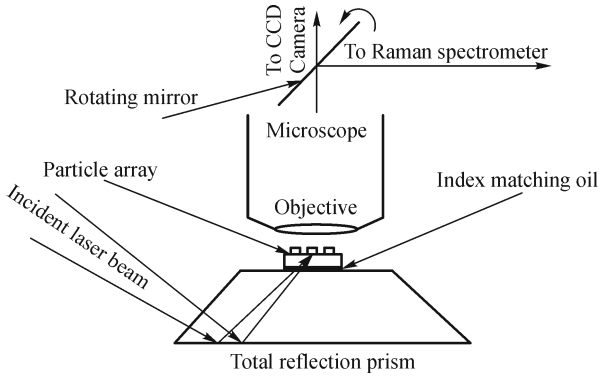

Figure 13 Optical input scheme for TIR excitation of the localized plasmon at the nanoparticle array/air interface. Reprinted with permission from Ref. [61]. Copyright©2005 American Chemical Society

direction (in the Kretschmann cone). They found that the fraction of the collected Kretschmann cone depends linearly on the NA.

Similar to the configuration as above, in our ongoing study, the Raman scattering can be focused and collected in the other resonant direction (as shown in Fig. 12). In this configuration, the twofold EM mechanism of SERS can be separated [60]. Since the back-coupled radiation of SPs is a reverse process of SPR, the radiation of SERS was directional and the radiation angle exactly matched the SPR angles. The experimental results showed that the maximal SERS enhancement was achieved when the incident angle was tuned to the SPR angle. The space distribution of SERS in the Kretschmann configuration clearly presented that the directional SERS owned a small divergence angle of less 3°. The directional SERS on the prism side was about ten times stronger than the scattering on the air side.

2.2 SERS based on waveguide-coupling SPR configurations

Waveguide coupling mode is built through the traditional waveguide configurations modified with metal layers. SPs were excited at the boundaries of waveguide configurations in the evanescent field. At the same time, waveguide substances can collect the re-coupled SPs and transfer the optical information with less transmission loss due to the total internal reflection (TIR) form. So the SPs in waveguides own longer path length.

Le'vi et al. [61] excited SERS on a single layer of gold nanoparticle periodic arrays using a TIR prism (Fig. 13). The SERS spectra and images were recorded in the same spatial and spectral regions and displayed circular spots spaced by the grating constant. It is interesting that these Raman scattering images can reflect the location of the gold nanoparticles with the sizes defined by the diffraction limit.

Li and Sun et al. [62] excited SERS using an evanescent wave propagating in a quasi-one-dimensional MoO_3 ribbon dielectric waveguide (Fig. 14). Probes adsorbed silver nanoparticles on the MoO_3 ribbon were excited by the evanescent wave propagated 7.3 μm in the MoO_3 ribbon. Clear Raman signals were obtained at a distant location on the dielectric waveguide where the adjacent silver nanoparticles were laid. Both the charge transfer and EM enhancement were achieved and discussed in this model.

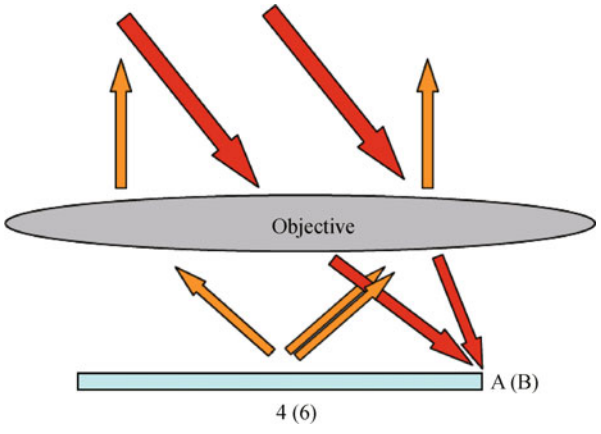

Figure 14 Scheme of the remote SERS measurement using a quasi-one-dimensional ribbon dielectric waveguide, where A and B stand for the point that laser radiates on the edge of ribbon belt and collection point of SERS, and the red and brown arrows stands for the incident and scattering and collection SERS signal, respectively. Reprinted with permission from Ref. [62]. Copyright©2011 Springer Science + Business Media

To highly integrate waveguide and coupling lens, optical fibers were frequently employed. For obtaining high SERS activity, they were decorated by a metal layer with reasonable roughness. Analytes on the SERS-active layer were excited by

the evanescent field and the scattering signals were collected by the fiber waveguide. In these cases, a single fiber was enough for the construction of an SERS-active optical sensor. By using these SERS-active optical fibers, the detection limit could reach 10^{-9} mol/L [63]. Methods for the fabrication of SERS-active layers on the distal ends of the SERS-active optical fiber sensors are various, e.g., vacuum deposited silver island [63–66], self-assembled silver colloid [63,67], and light-induced silver deposition (Fig. 15) [68]. In recent reports, a gold optical antennas array [69] and a gold grid nanostructure [70] were fabricated on the distal ends of optical fibers to provide more hot spots and doubly resonant SPs.

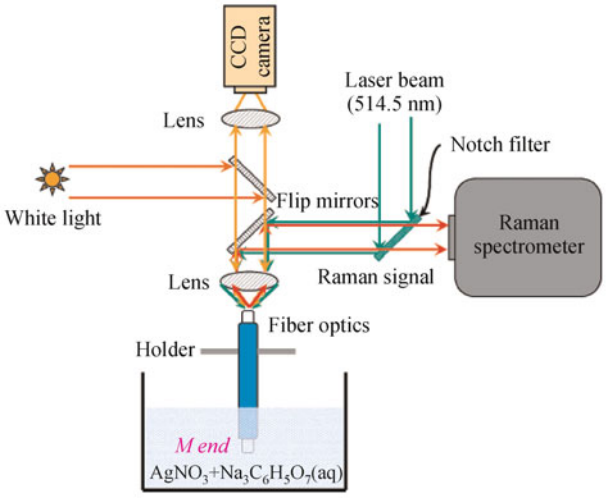

Figure 15 Schematic diagram of an SERS-active optical fiber. Reprinted with permission from Ref. [68]. Copyright©2008 American Chemical Society

The geometry of the fiber tips was optimized for the best coupling of waveguides [71]. Hill et al. [72,73] optimized the SP coupling by changing the shape of fiber tips with different shapes. They polished the terminal end to form angled tips. The angled tip enlarged the vector moment of the electric field in the perpendicular direction and excited the largest SPs at ~45°. The SERS signals obtained on a 40° angled tip was 6 times stronger than those on a 0° angled tip.

Gu et al. [74] proposed a D-shaped fiber configuration to increase detection area (Fig. 16). They modified an SERS-active layer on a polished fiber side face and found most of the light could be absorbed by the modified layer. A several orders of magnitude extension in surface area led to substantially more detectable Raman scattered photons than those in end-tip configurations.

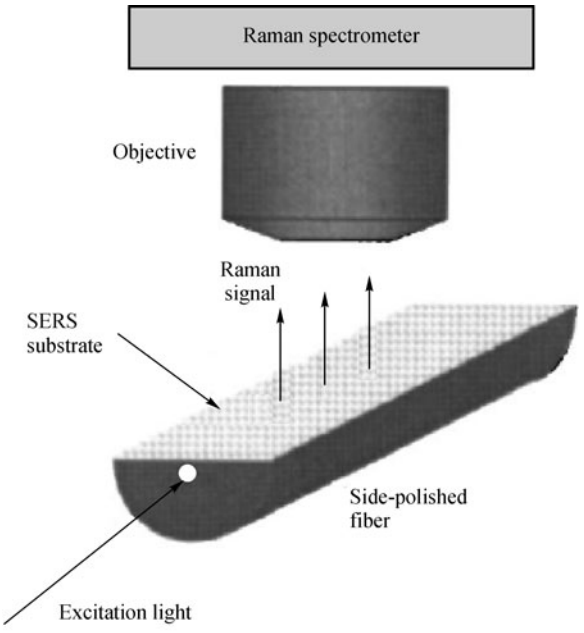

Figure 16 Schematic of the Raman probe with a D-shaped (or side-polished) fiber coated with SERS substrate on the flat surface. Reprinted with permission from Ref. [74]. Copyright©2005 American Institute of Physics

SERS signals can be further improved by using the ATR mode in a liquid core (LC) fiber. Xu et al. [75] reports an SERS-active LC waveguide method for ultrasensitive detection of a sample dissolved in a small volume of low refractive index liquid. The SERS-active LC fiber demonstrated was constructed via the surface modification of SERS-active silver nanoparticles on the inner wall of the light-guiding silica capillary (Fig. 17). The incident laser beam traveled through the waveguide in an ATR mode within the fiber wall and penetrated a small distance into the sample solution by the evanescent field. Thus, a sample dissolved in

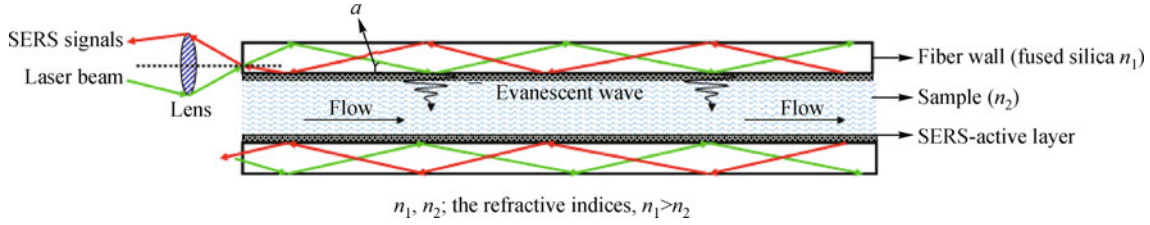

Figure 17 Configuration of SERS-active light waveguide applied to the SERS detection of a sample in a small volume of low refractive index liquid. Reprinted with permission from Ref. [75]. Copyright©2004 Optical Society of America

low refractive index liquid could be quantitatively monitored by Raman spectroscopy, and the detection limit of its concentration was lower than 10^{-9} mol/L due to multi-reflection.

Photonic crystal optical fiber is a kind of special and powerful optical fibers with periodic arrangement of air holes, which owns the unique guiding properties based on TIR and photonic bandgaps. In a photonic crystal optical fiber, the spectral and temporal characteristics of the guided light can be engineered. Gu [76] and Sazio [77] modified the inner surface of hollow core photonic crystal optical fibers with metal nanoparticles serving as the multi-channel SERS optical sensors (Fig. 18). Their design offered a large area for the light to interact with the SERS-active nanoparticles, which further improved the probe sensitivity. Yan et al. [78] further used a kind of index-guided photonic crystal fiber with four big air holes inserted between the solid silica core and the photonic crystal cladding holes in order to construct a SERS optical sensor. Due to the special design of the optical fiber, the light was confined inside the solid core, which resulted in the energy overlap factor as high as 21.45% from the simulated results.

3 SERS based on grating-coupling SPR configurations

Grating coupling SPR is another commonly used configuration based on the metal substrates with periodicity. Tuning the parameter of periodicity can effectively control SPs. On these grating type substrates, the emission of SERS was directional, and strong SERS was obtained only at defined detection angles. This directional SERS was attributed to the SP-coupled emission on grating structures.

The coupling theory of SPs and light on periodical metal surface is briefly introduced here. For a grating type SPR sensor, periodical factor introduces an extra momentum, which causes the matching of the incident light and SP. The wave vector of the SP can be expressed by the following Eq. (6).

$$\vec{k} = \frac{2\pi}{\lambda}\sqrt{\frac{\varepsilon_m \varepsilon_{air}}{\varepsilon_m + \varepsilon_{air}}}\nu + n\frac{2\pi}{a}i + m\frac{2\pi}{a}j \qquad (6)$$

where λ is the free space wavelength, ε_{air} and ε_m are the dielectric functions of air and metal, a is the period in both x- and y-directions, and n and m are integers. k is the in-plane wave vector of the incident field, which is related to the incident angle $\left(k = \frac{2\pi}{\lambda}\sin\theta\right)$, υ is the unit vector along the propagating direction of the excited SPs, and finally, i and j are the unit vectors along the x- and y-axes [79].

In 1980s, SERS on metal gratings were reported [80–82]. SERS of pyridine on a clean single-crystal silver surface containing 1 μm periodicity was recorded, and it indicated the optical coupling to SPs. An EF of ~10^4 of the Raman signal was observed under SPR condition [80].

With the development of microfabrication techniques, the designs of periodical SERS substrates extended from one-dimensional gratings to two-dimensional arrays. Kahl and Voges [83] calculated the EM near field for rectangular-

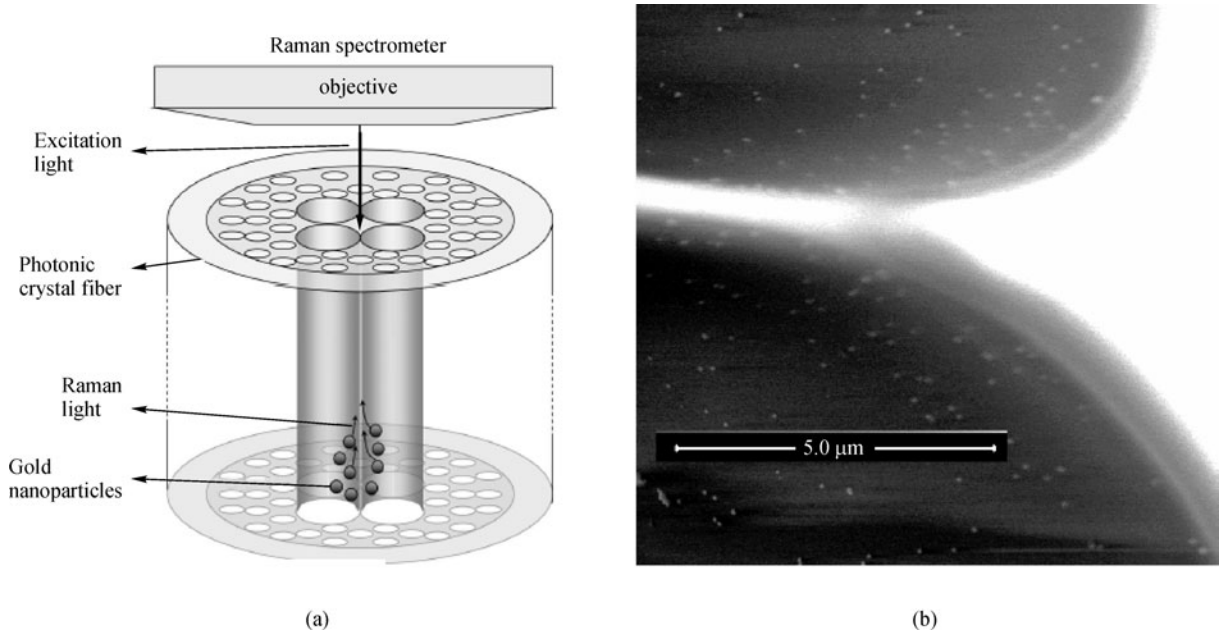

Figure 18 (a) Schematic of the experimental setup. (b) SEM image taken from the side surface of the silica core. Reprinted with permission from Ref. [78]. Copyright©2008 Optical Society of America

groove gratings and the far field signals of Raman-active molecules adsorbed at the grating surfaces with different geometries. SERS EFs were considered to be between 10 and 10^5 depending on both the grating structures and the experimental configurations. SERS signals were maximally enhanced at the shallow gratings with depths between 10 and 20 nm, and an emission angle that corresponded to the SPR angle at the Stokes wavelength. SERS signals from deep gratings were emitted into a larger angular range and the optimum grating depths of more than 80 nm were suggested.

Another example of periodical SERS substrate design was to consider the PSPs and LSPs co-enhancement effect. Mei et al. [84] investigated the plasmonic properties of the two-dimensional dielectric grating covered by a silver film with a thickness of tens of nanometers for a SERS substrate, on which both the LSPs and SPPs can be excited for a considerable boost of Raman enhancement (Fig. 19). For the LSPs, the resonance wavelength was affected by the distance between bumps. For large structural period, meaning that bumps were separated far away, the plasmon resonance wavelength shift resulted from the long-range interactions. A Raman enhancement of ~2 × 10^9 was achieved in the proposed structure.

The design of SERS substrates in consideration of plasmonic band gap was proposed by Aydinli et al. [85] They worked on the SERS spectra of rhodamine 6G (R6G) adsorbed on biharmonic metal grating structures (Fig. 20), which were prepared by the soft nano-imprint technique. Biharmonic metal gratings included two different grating components, one acting as a coupler to excite SPs, and the other forming a plasmonic band gap for PSPs. These localized plasmons strongly enhance the scattering efficiency of the Raman signal emitted on the metal grating surfaces. The reproducible Raman scattering EF was achieved as over 10^5. They also showed that the SERS activities from these templates were tunable as a function of plasmonic resonance conditions.

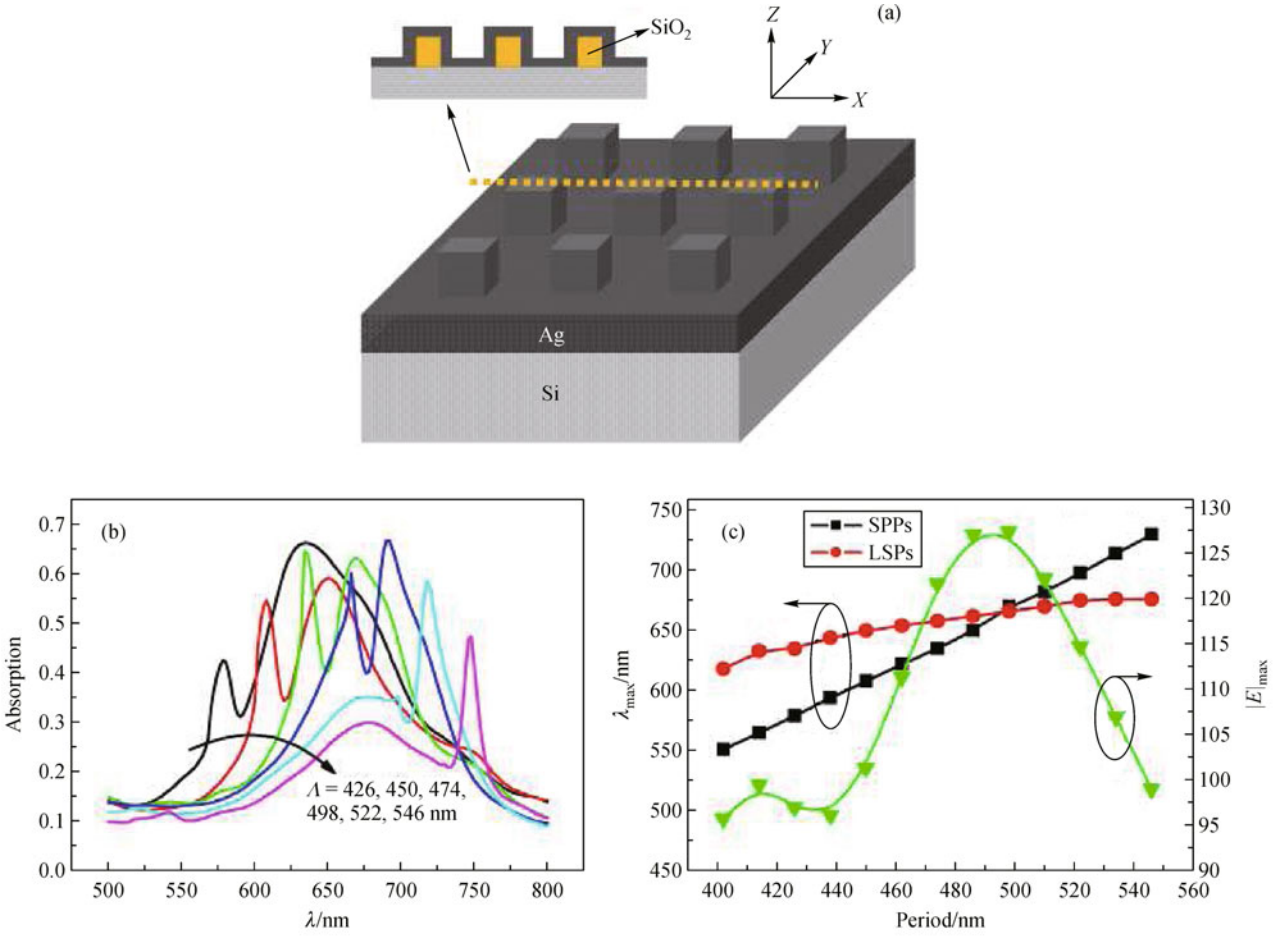

Figure 19 (a) A proposed wo-dimensional SERS grating structure and its spectral properties; (b) Absorption spectra for various periods from 426 to 546 nm with a 24 nm increment; (c) absorption peak positions versus different periods for LSPs (circles) and SPPs (squares), with corresponding maximum local $|E|$ at resonance wavelength of SPPs (triangles). The silver film thickness was 40 nm, the bump height was 100 nm and the environment is water. Reprinted with permission from Ref. [84]. Copyright©2010 Optical Society of America

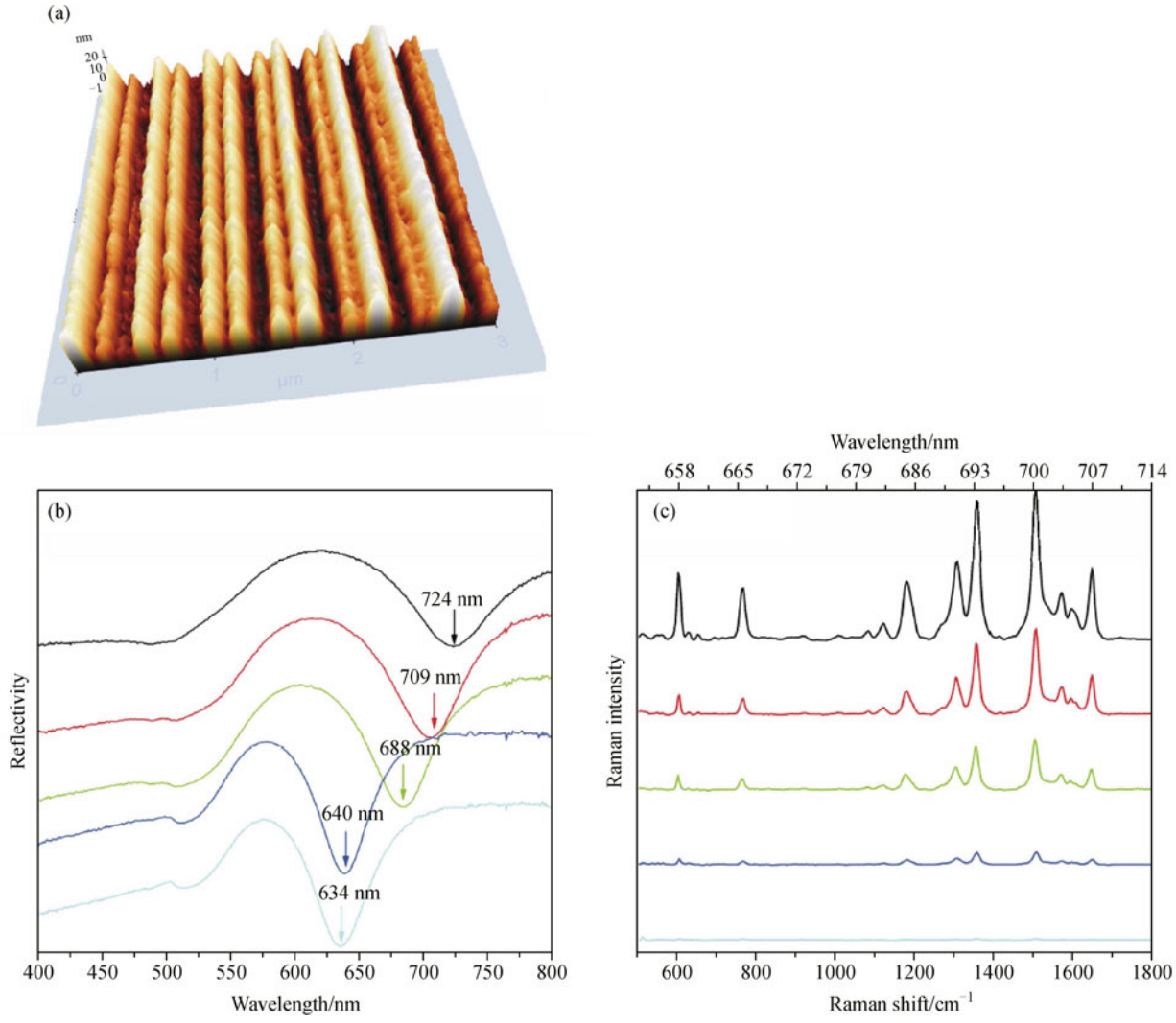

Figure 20 (a) An AFM image of biharmonic metal surface with the grating components of 500 and 250 nm. First periodicity was designed to excite the SPs. Second one generated backscattering for PSPs with a photonic band gap. (b) Resonance absorption spectra of biharmonic metal gratings with different grating strengths; (c) Corresponding SERS spectra for each resonance condition. Reprinted with permission from Ref. [85]. Copyright©2008 Optical Society of America

Baumberg et al. [79] used a templating method to produce a periodic array of spherical void in metal film for studying the directional SERS emission (Fig. 21). By mapping the SERS signal at different angles of both the incident pump laser and the emitted Raman photons, they demonstrated clearly the resonant plasmon enhancement of SERS signals. The EF from the gold void array was about 3×10^6. Sharp enhancements occurred when the laser was scanned through a plasmon resonance (ingoing process) and also when individual Raman scattered lines coincided with plasmon resonances (outgoing process). Moreover, they attributed the ingoing and outgoing resonances to different plasmons.

Similar work was reported by Ong et al. [86]. They studied the angle-resolved SERS on two-dimensional Ag hole arrays as a function of hole size. The Raman EF was found to increase with the hole size. In particular, by correlating the Raman mappings with the dispersion relations, the enhancement was attributed to a fast SPP radiative decay rate and strong coupling efficiency.

One of the important advantages of periodical SERS substrates is that they support higher reproducibility in SERS detections than metal nanoparticles or nanoaggregates do. Many literatures tried to design novel micro and nano periodical metal structures for the purposes of not only good reproducibility but also high enhancement. In recent study, Hu and Zou et al. [87] employed the numerical simulations to analyze the optical properties of the periodic arrays of nanoscale cavities in thin silver films to demonstrate the possibility of creating controllable hot spots through tuning cavity geometry, film thickness, and array period.

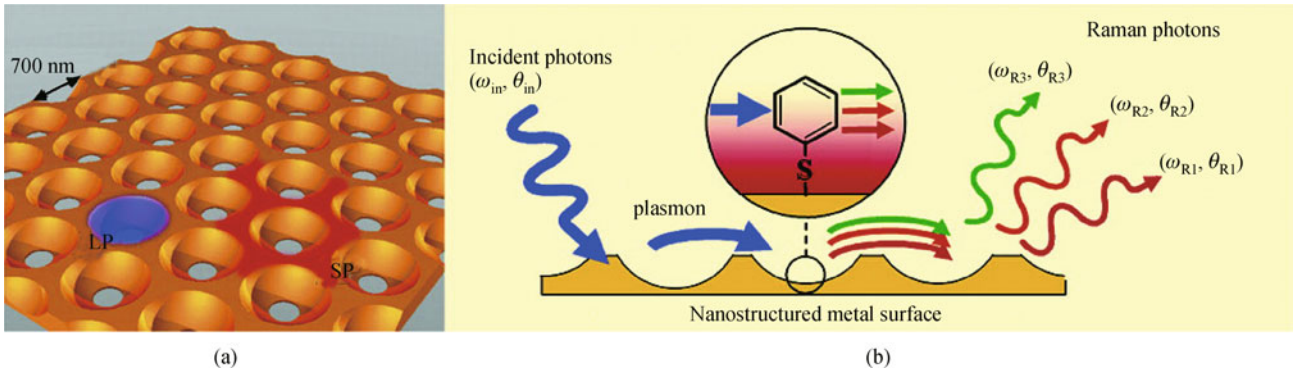

Figure 21 Schematic metal nanostructured plasmonic crystals (b) schematic SERS process; light is coupled into a plasmon, which then interacts with and is Raman scattered by a molecule on the surface, and the outgoing plasmon is then scattered back into a photon. Emitted far-field Raman images deduced from the measured plasmonic nanovoid extinction for (a) propagating and (b) localized plasmons. Reprinted with permission from Ref. [79]. Copyright©2005 American Chemical Society

4 Prospective

With a deeper insight into the plasmonic devices and nanoantennas, optical devices for coupling the excitation and radiation of SERS become ingenious and integrative. The strong integration of functional components, e.g., light path, coupling lens, and sampling stage, etc., simplifies the instruments for SERS. The utlization of optical fibers and microfluidics realizes "lab on chip". A trend of micromation of SERS setups is taking form and becomes promising.

The implanting of the near field configurations is expected to be another promising way for improving SERS techniques. For example, the utilization of high NA lens [26–28] and nanojet configurations [88,89] would be very interesting for SERS excitation and collection. The trend of this study strongly depends on the progress of plasmonics. At micro and nano scales, special behaviors and performances about SERS would be disclosed by using the near field techniques.

Opportunities and challenges both exist in the studies of SERS substrates for the lasting purposes of higher enhancement and better reproducibility. The micro-machining technique is always supporting the development of two- and three-demensional SERS substrates. The effective coupling of SPs is still a key point for various SERS substrates.

References

1. Fleischmann, M.; Hendra, P. J.; McQuilla, A. J., *Chem. Phys. Lett*. **1974**, *26*, 163–166
2. Chang, R. K.; Furtak, T. E., eds., Surface-Enhanced Raman Scattering, *Plenum Press, New York*, *1982*.
3. Jeanmaire, D. L.; Van Duyne, P. R., *J. Electroanal. Chem*. **1977**, *84*, 1–20
4. Kerker, M., ed., Selected Papers on Surface-Enhanced Raman Scattering, *SPIE, Bellingham, WA*, *1990*.
5. Kneipp, K.; Kneipp, H.; Itzkan, I.; Dasari, R. R.; Feld, M. S., *Chem. Rev*. **1999**, *99*, 2957–2976
6. Schatz, G. C.; Van Duyne, P. R., Handbook of Vibrational Spectroscopy Vol. 1: Electromagnetic Mechanism of Surface-Enhanced Spectroscopy, *Chalmers, J. M., Griffiths, P. R, (Eds)*; *John Wiley & Sons Ltd., Chichester, U.K*., *2002*, pp 759–774
7. Kneipp, K.; Moskovits, M.; Kneipp, H., eds., Surface-Enhanced Raman Scattering- Physics and Applications, *Springer, Heidelberg and Berlin*, *2006*
8. Graham, D.; Goodacre, R., *Chem. Soc. Rev*. **2008**, *37*, 883–884
9. Aroca, R., ed., Surface-Enhanced Vibrational Spectroscopy, John Wiley & Sons Ltd., Chichester, UK, 2006, pp. 141–176
10. Nie, S.; Emory, S. R., *Science* **1997**, *275*, 1102–1106
11. Kneipp, K.; Wang, Y.; Kneipp, H.; Perelman, L. T.; Ltzkan, I.; Dasari, R. R.; Feld, M. S., *Phys. Rev. Lett*. **1997**, *78*, 1667–1670
12. Xu, H. X.; Bjerneld, E. J.; Käll, M.; Börjesson, L., *Phys. Rev. Lett*. **1999**, *83*, 4357–4360
13. Ekgasit, S.; Thammacharoen, C.; Yu, F.; Knoll, W., *Anal. Chem*. **2004**, *76*, 2210–2219
14. Brolo, A. G.; Kwok, S. C.; Moffitt, M. G.; Gordon, R.; Riordon, J.; Kavanagh, K. L., *J. Am. Chem. Soc*. **2005**, *127*, 14936–14941
15. Lakowicz, J. R.; Ray, K.; Chowdhury, M.; Szmacinski, H.; Fu, Y.; Zhang, J.; Nowaczyk, K., *Analyst (Lond.)* **2008**, *133*, 1308–1346
16. Hatta, A.; Ohshima, T.; Suetaka, W., *Appl. Phys., A Mater. Sci. Process*. **1982**, *29*, 71–75
17. Ebbesen, T. W.; Lezec, H. J.; Ghaemi, H. F.; Thio, T.; Wolff, P. A., *Nature* **1998**, *391*, 667–669
18. Xu, H. X.; Aizpurua, J.; Käll, M.; Apell, P., *Phys. Rev. E Stat. Phys. Plasmas Fluids Relat. Interdiscip. Topics* **2000**, *62*, 4318–4324
19. Johansson, P.; Xu, H. X.; Käll, M., *Phys. Rev. B* **2005**, *72*, 035427
20. Moskovits, M., *Rev. Mod. Phys*. **1985**, *57*, 783–826
21. Schatz, G. C.; Young, M. A.; Van Duyne, R. P., *Topics in Applied Physics 103*, 19–45
22. Yoshida, K.; Itoh, T.; Tamaru, H.; Biju, V.; Ishikawa, M.; Ozaki,

Y., *Phys. Rev. B* **2010**, *81*, 115406
23. Itoh, T.; Hashimoto, K.; Ikehata, A.; Ozaki, Y., *Appl. Phys. Lett*. **2003**, *83*, 5557–5559
24. Itoh, T.; Hashimoto, K.; Ozaki, Y., *Appl. Phys. Lett*. **2003**, *83*, 2274–2276
25. McFarland, A. D.; Young, M. A.; Dieringer, J. A.; Van Duyne, R. P., *J. Phys. Chem. B* **2005**, *109*, 11279–11285
26. Bouhelier, A.; Wiederrecht, G. P., *Opt. Lett*. **2005**, *30*, 884–886
27. Shegai, T.; Brian, B.; Miljković, V. D.; Käll, M., *ACS Nano* **2011**, *5*, 2036–2041
28. Kosemura, D.; Ogura, A., *Appl. Phys. Lett*. **2010**, *96*, 212106
29. Hayazawa, N.; Saito, Y.; Kawata, S., *Appl. Phys. Lett*. **2004**, *85*, 6239
30. Ren, B.; Picardi, G.; Pettinger, B.; Schuster, R.; Ertl, G., *Angew. Chem. Int. Ed*. **2005**, *44*, 139–142
31. Liu, Z.; Ding, S. Y.; Chen, Z. B.; Wang, X.; Tian, J. H.; Anema, J. R.; Zhou, X. S.; Wu, D. Y.; Mao, B. W.; Xu, X.; Ren, B.; Tian, Z. Q., *Nature Commun*. **2011**, *2*, 305
32. Hansen, W. N., *J. Opt. Soc. Am*. **1968**, *58*, 380–390
33. Ekgasit, S.; Thammacharoen, C.; Knoll, W., *Anal. Chem*. **2004**, *76*, 561–568
34. Dornhaus, R.; Benner, R. E.; Chang, R. K.; Chabay, I., *Surf. Sci*. **1980**, *101*, 367–373
35. Giergiel, J.; Reed, C. E.; Hemminger, J. C.; Ushioda, S., *J. Phys. Chem*. **1988**, *92*, 5357–5365
36. Yih, J. N.; Chen, S. J.; Huang, K. T.; Su, Y. T.; Lin, G. Y., *Proc. SPIE* **2004**, *5327*, 5–9
37. Liu, Y.; Xu, S. P.; Tang, B.; Wang, Y.; Zhou, J.; Zheng, X. L.; Zhao, B.; Xu, W. Q., *Rev. Sci. Instrum*. **2010**, *81*, 036105
38. Hu, W. P.; Chen, S. J.; Yih, J. N.; Lin, G. Y.; Chang, G. L., *Proc. SPIE* **2004**, *5327*, 88–94
39. Chiu, K. C.; Yu, L. Y.; Yih, J. N.; Chen, S. J., *Proc. SPIE* **2007**, *6450*, 64500R
40. Giergiel, J.; Reed, C. E.; Hemminger, J. C.; Ushioda, S., *J. Phys. Chem*. **1988**, *92*, 5357–5365
41. Kocabas, A.; Ertas, G.; Senlik, S. S.; Aydinli, A., *Opt. Express* **2008**, *17*, 12469–12477
42. Zhou, Q.; Li, X. W.; Fan, Q.; Zhang, X. X.; Zheng, J. W., *Angew. Chem. Int. Ed*. **2006**, *45*, 3970–3973
43. Orendorff, C. J.; Gole, A.; Sau, T. K.; Murphy, C. J., *Anal. Chem*. **2005**, *77*, 3261–3266
44. Daniels, J. K.; Chumanov, G., *J. Phys. Chem. B* **2005**, *109*, 17936–17942
45. Kim, K.; Yoon, J. K., *J. Phys. Chem. B* **2005**, *109*, 20731–20736
46. Liu, Y.; Xu, S. P.; Li, H. B.; Jian, X. G.; Xu, W. Q., *Chem. Commun. (Camb.)* **2011**, *47*, 3784–3786
47. Sarid, D., *Phys. Rev. Lett*. **1981**, *47*, 1927–1930
48. Craig, A. E.; Olson, G. A.; Sarid, D., *Opt. Lett*. **1983**, *8*, 380–382
49. Matsubara, K.; Kawata, S.; Minami, S., *Opt. Lett*. **1990**, *15*, 75–77
50. Yang, F.; Bradberry, G. W.; Sambles, J. R., *Phys. Rev. Lett*. **1991**, *66*, 2030–2032
51. Kessler, M. A.; Hall, E. A. H., *Thin Solid Films* **1996**, *272*, 161–169
52. Lyndin, N. M.; Salakhutdinov, I. F.; Sychugov, V. A.; Usievich, B. A.; Pudonin, F. A.; Parriaux, O., *Sens. Actuators B Chem*. **1999**, *54*, 37–42
53. Toyama, S.; Doumae, N.; Shoji, A.; Ikariyama, Y., *Sens. Actuators B Chem*. **2000**, *65*, 32–34
54. Nenninger, G. G.; Tobiska, P.; Homola, J.; Yee, S. S., *Sens. Actuators B Chem*. **2001**, *74*, 145–151
55. Liu, Y.; Xu, S. P.; Xuan, X. Y.; Zhao, B.; Xu, W. Q., *J. Phys. Chem. Lett* **2011**, *2*, 2218–2222
56. Futamata, M., *Appl. Opt*. **1997**, *36*, 364–375
57. Futamata, M.; Borthen, P.; Thomassen, J.; Schumacher, D.; Otto, A., *Appl. Spectrosc*. **1994**, *48*, 252–260
58. Futamata, M., *Langmuir* **1995**, *11*, 3894–3901
59. Meyer, S. A.; Le Ru, E. C.; Etchegoin, P. G., *Anal. Chem*. **2011**, *83*, 2337–2344
60. Itoh, T.; Yoshida, K.; Biju, V.; Kikkawa, Y.; Ishikawa, M.; Ozaki, Y., *Phys. Rev. B* **2007**, *76*, 085405
61. Laurent, G.; Félidj, N.; Truong, S. L.; Aubard, J.; Lévi, G.; Krenn, J. R.; Hohenau, A.; Leitner, A.; Aussenegg, F. R., *Nano Lett*. **2005**, *5*, 253–258
62. Dong, B.; Zhang, W.; Li, Z. P.; Sun, M. T., *Plasmonics* **2011**, *6*, 189–193
63. Xu, W. Q.; Xu, S. P.; Hu, B.; Wang, K. X.; Zhao, B.; Xie, Y. T.; Fan, Y. G., *Chem. Res. Chin. Univ*. **2004**, *1*, 144–147
64. Mullen, K. I.; Carron, K. T., *Anal. Chem*. **1991**, *63*, 2196–2199
65. Viets, C.; Hill, W., *Sens. Actuators B Chem*. **1998**, *51*, 92–99
66. Stokes, D. L.; Chi, Z.; Vo-Dinh, T., *Appl. Spectrosc*. **2004**, *58*, 292–298
67. Polwart, E.; Keir, R. L.; Davidson, C. M.; Smith, W. E.; Sadler, D. A., *Appl. Spectrosc*. **2000**, *54*, 522–527
68. Zheng, X. L.; Guo, D. W.; Shao, Y. L.; Jia, S. J.; Xu, S. P.; Zhao, B.; Xu, W. Q.; Corredor, C.; Lombardi, J. R., *Langmuir* **2008**, *24*, 4394–4398
69. Smythe, E. J.; Dickey, M. D.; Bao, J.; Whitesides, G. M.; Capasso, F., *Nano Lett*. **2009**, *9*, 1132–1138
70. Tian, M.; Lu, P.; Schülzgen, A.; Peyghambarian, N.; Liu, D., *Opt. Commun*. **2011**, *284*, 2061–2064
71. Lucotti, A.; Zerbi, G., *Sens. Actuators B Chem*. **2007**, *121*, 356–364
72. Kostrewa, S.; Hill, W.; Klockow, D., *Sens. Actuators B Chem*. **1998**, *51*, 292–297
73. Viets, C.; Hill, W., *J. Raman. Spectrosc.* **2000**, *31*, 625–631
74. Zhang, Y.; Gu, C.; Schwartzberg, A. M.; Zhang, J. Z., *Appl. Phys. Lett*. **2005**, *87*, 123105
75. Xu, W. Q.; Xu, S. P.; Lu, Z. C.; Chen, L.; Zhao, B.; Ozaki, Y., *Appl. Spectrosc*. **2004**, *58*, 414–419
76. Yan, H.; Gu, C.; Yang, C. X.; Liu, J.; Jin, G. F.; Zhang, J. T.; Hou, L. T.; Yao, Y., *Appl. Phys. Lett*. **2006**, *89*, 204101
77. Amezcua-Correa, A.; Yang, J.; Finlayson, C. E.; Peacock, A. C.; Hayes, J. R.; Sazio, P. J. A.; Baumberg, J. J.; Howdle, S. M., *Adv. Funct. Mater*. **2007**, *17*, 2024–2030
78. Yan, H.; Liu, J.; Yang, C. X.; Jin, G. F.; Gu, C.; Hou, L. T., *Opt. Express* **2008**, *16*, 8300–8305

79. Baumberg, J. J.; Kelf, T. A.; Sugawara, Y.; Cintra, S.; Abdelsalam, M. E.; Bartlett, P. N.; Russell, A. E., *Nano Lett*. **2005**, *5*, 2262–2267
80. Sanda, P. N.; Warlaumont, J. M.; Demuth, J. E.; Tsang, J. C.; Christmann, K.; Bradley, J. A., *Phys. Rev. Lett*. **1980**, *45*, 1519–1523
81. Otto, A., *Appl. Surf. Sci*. **1980**, *6*, 309–355
82. Liao, P. F.; Bergman, J. G.; Chemla, D. S.; Wokaun, A.; Melagailis, J.; Hawryluk, A. M.; Economou, N. P., *Chem. Phys. Lett*. **1981**, *82*, 355–359
83. Kahl, M.; Voges, E., *Phys. Rev. B* **2000**, *61*, 14078–14088
84. Du, L.; Zhang, X.; Mei, T.; Yuan, X., *Opt. Express* **2010**, *18*, 1959–1965
85. Kocabas, A.; Ertas, G.; Senlik, S. S.; Aydinli, A., *Opt. Express* **2008**, *16*, 12469–12477
86. Chan, C. Y.; Xu, J. B.; Waye, M. Y.; Ong, H. C., *Appl. Phys. Lett*. **2010**, *96*, 033104
87. Hu, W. F.; Zou, S. L., *J. Phys. Chem. C* **2011**, *115*, 4523–4532
88. Bouhelier, A.; Wiederrecht, G. P., *Opt. Lett*. **2005**, *30*, 884–886
89. Dantham, V. R.; Bisht, P. B.; Namboodiri, C. K. R., *J. Appl. Phys*. **2011**, *109*, 103103